Inhibition of circRNA circVPS33B reduces cell malignant behaviors and Warburg effect through regulation of the miR-873-5p/HNRNPK axis in infiltrative gastric cancer

Yizhuo Lu
Zhongshan Hospital of Xiamen University
Jia Cheng
Zhongshan Hospital of Xiamen Univeristy
Wangyu Cai
Zhongshan Hospital of Xiamen University
Huiqin Zhuo
Zhongshan Hospital of Xiamen University
Guoyang Wu
Zhongshan Hospital of Xiamen University
Jianchun Cai (jianchuncai0592@163.com)
Zhongshan Hospital of Xiamen University https://orcid.org/0000-0001-9234-4350

Primary research

Keywords: CircVPS33B, miR-873-5p, HNRNPK, infiltrative GC

Posted Date: July 20th, 2020

DOI: https://doi.org/10.21203/rs.3.rs-43509/v1

Abstract

Background

Circular RNA VPS33B (circVPS33B) is upregulated in gastric cancer (GC) tissues. However, the role of circVPS33B in infiltrative GC is indistinct.

Methods

Expression of circVPS33B, miR-873-5p, and heterogeneous nuclear ribonucleoprotein K (HNRNPK) mRNA was detected using quantitative real-time polymerase chain reaction (qRT-PCR). The proliferation, colony formation, migration, and invasion of infiltrative GC cells (XGC-1) were determined by 3-(4,5-dimethylthiazol-2-yl)-2,5-diphenyltetrazoliumbromide (MTT), plate clone, wound healing, or transwell assays. Several protein levels were examined by western blotting. The extracellular acidification rate (ECAR) and oxygen consumption rate (OCR) of XGC-1 cells were evaluated by XF96 extracellular flux analyzer. Glucose uptake and lactate production were analyzed by glycolysis assay. The relationship between circVPS33B or HNRNPK and miR-873-5p was verified by dual-luciferase reporter and/or RNA pull-down assays. *In vivo* tumorigenesis assay was executed for verifying the *in vitro* results.

Results

CircVPS33B and HNRNPK were upregulated while miR-873-5p was downregulated in infiltrative GC tissues and XGC-1 cells. CircVPS33B silencing decreased tumor growth *in vivo* and inhibited proliferation, colony formation, migration, invasion, and Warburg effect of XGC-1 cells *in vitro*. CircVPS33B regulated HNRNPK expression via sponging miR-873-5p. The inhibitory influence of circVPS33B knockdown on the malignancy and Warburg effect of XGC-1 cells was overturned by miR-873-5p inhibitor. HNRNPK overexpression reversed the repression of the malignancy and Warburg effect of XGC-1 cells caused by miR-873-5p mimic.

Conclusions

CircVPS33B accelerated infiltrative GC progression through regulating the miR-873-5p/HNRNPK axis, manifesting that circVPS33B might be a promising target for infiltrative GC treatment.

Highlights

1. CircVPS33B expression was elevated in infiltrative GC tissues and XGC-1 cells.
2. Downregulation of circVPS33B reduced the malignancy and Warburg effect of XGC-1 cells.
3. CircVPS33B acted as a sponge for miR-873-5p in XGC-1 cells.

4. HNRNPK served as a target for miR-873-5p in XGC-1 cells.
5. The study provided a new mechanism to understand the progression of infiltrative GC.

Background

Gastric cancer (GC), a malignant tumor that occurs in the stomach, ranks third among cancer-related death causes [1]. GC is divided into infiltrative and expanding types according to the growth and invasive patterns based on Ming's classification [2]. Moreover, the prognosis of infiltrative GC is worse than that of expanding GC [3]. Studies have reported that the recurrence of the peritoneal or liver after radical resection of GC is closely related to the pathological infiltrative pattern (INF) [4, 5]. Therefore, it is of great significance to explore the latent molecular mechanism of infiltrative GC progression.

Circular RNAs (circRNAs), endogenous non-coding RNAs, have closed-loop structures formed by reverse splicing of mRNA exons or introns [6]. They are more stable than other conventional linear RNAs due to their resistance to exonucleases [7]. Studies have revealed that circRNAs exert diverse vital roles in cellular physiology through serving as protein translation templates, transcription regulators, RBP-binding molecules, or microRNA (miR) sponges [8]. Also, circRNAs dysregulation are closely related to the advancement of diverse diseases, including cancers [9]. For example, circRNA hsa_circ_0003141 contributed to the tumorigenesis of hepatocellular cancer [10]. CircRNA VPS33B, also termed as hsa_circ_0005529, is derived from the vacuolar protein sorting 33 homologue B (VPS33B) gene. It was reported that circVPS33B was elevated in GC tissues (GSE78092) [11]. However, the role of circVPS33B in infiltrative GC progression is unclear.

MiRs can regulate the expression of genes via binding to the 3' Untranslated Regions (UTR) of target mRNAs [12]. They act as powerful regulatory factors in a series of cellular activities, including cell development, differentiation, growth, and apoptosis [13]. It has been revealed that miRs exert important roles in numerous cases of cancers [14]. For instance, the miR-34 family served as potential therapeutic candidates in cancers [15]. It was reported that miR-873-5p acted as an epigenetic modulator in the early stages of liver fibrosis and cirrhosis [16]. Studies have shown that miR-873-5p played an inhibitory role in numerous cancers development, such as glioma [17], papillary thyroid cancer [18], and colorectal cancer [19]. Moreover, miR-873-5p was uncovered to curb the malignancy of GC cells [20, 21]. However, the mechanism of miR-873-5p in infiltrative GC progression has not been fully clarified.

Heterogeneous nuclear ribonucleoprotein K (HNRNPK), a DNA/RNA-binding protein, is involved in regulating various biological processes and disease pathogenesis [22]. Previous study manifested that HNRNPK inhibition could elevate DNA damage after radiation, thereby decreasing the survival of tumor cells [23]. Moreover, high HNRNPK level is related to poor prognosis and development in several cancers, such as bladder cancer [24] and colorectal cancer [25]. HNRNPK was also revealed to facilitate the progression of GC [26]. Nevertheless, the mechanisms associated with HNRNPK in infiltrative GC development are relatively less known.

In the present study, we verified circVPS33B played a stimulative role in infiltrative GC advancement. Moreover, circVPS33B inhibition reduced the malignancy and Warburg effect of infiltrative GC cells via downregulating HNRNPK through competitively binding to miR-873-5p. Our findings provided a novel mechanism that circVPS33B modulated infiltrative GC development through the miR-873-5p/HNRNPK axis.

Materials And Methods

Patient-derived samples

The research was approved by the Ethics Committee of the Ethics Committee of the Institute of Gastrointestinal Oncology, School of Medcine, Xiamen University. 37 paired infiltrative GC tissue samples and neighboring non-tumor tissues were collected from the Ethics Committee of the Institute of Gastrointestinal Oncology, School of Medcine, Xiamen University. None of the participating patients received other treatments before surgery. All participants signed written informed consents before starting this study.

Cell culture and transfection

Infiltrative GC cells XGC-1 (Patent No.: CN103396994A) was obtained from the Institute of Gastrointestinal Oncology, School of Medcine, Xiamen University (Xiamen, China). Human gastric epithelial mucosa cells (GES-1) was purchased from BeNa Culture Collection (Suzhou, China). These two cell lines were grown in Roswell Park Memorial Institute (RPMI)-1640 medium (HyClone, Logan, UT, USA) containing fetal bovine serum (FBS, 10%, HyClone) and streptomycin/penicillin (1%, Solarbio, Beijing, China) in a moist atmosphere with 5% CO_2 at 37˚C.

Small interference (si)-circVPS33B and negative control (si-NC), as well as short hairpin (sh)-circVPS33B and negative control (sh-NC), were purchased from GenePharma (Shanghai, China). For pcDNA-HNRNPK generation, the full-length sequence of HNRNPK was cloned into the empty pcDNA3.1 vector (pcDNA-NC) (Life Technologies, Grand Island, NY, USA). MiR-873-5p mimic (miR-873-5p), miR-873-5p inhibitor (anti-miR-873-5p), and their corresponding negative controls (miR-NC and anti-miR-NC) were purchased from RiboBio (Guangzhou, China). XGC-1 cells were transfected with vectors or oligonucleotides by Lipofectamine 3000 reagent (Invitrogen, Carlsbad, CA, USA). The stable circVPS33B knockdown cells were obtained by infecting with lentiviral particles and selecting with puromycin (Solarbio).

Quantitative real-time polymerase chain reaction (qRT-PCR)

RNAsimple Total RNA Kit from TIANGEN (Beijing, China) was utilized for total RNA separation (tissue samples and cells). The complementary DNA was synthesized with the M-MLV First Strand Kit (Life Technologies) or Bulge-Loop miR RT-qPCR Starter kit (RiboBio) and then used for qPCR with the SYBR Green (Solarbio). The primers were used as follows: circVPS33B (Forward: 5’-GTGGTGTTCTTGGGTGGTTGT-3’; Reverse: 5’-CCGCTCTAGCACCTTTCTCTC-3’), VPS33B (Forward: 5’-

ATGAGCCCTTTGGATCGAATTG-3’; Reverse: 5’-ATGCGGGGTCTGACCAAGA-3’), HNRNPK (Forward: 5’-CAATGGTGAATTTGGTAAACGCC-3’; Reverse: 5’-GTAGTCTGTACGGAGAGCCTTA-3’), β-actin (Forward: 5’-GCACCACACCTTCTACAATG-3’; Reverse: 5’-TGCTTGCTGATCCACATCTG-3’), miR-873-5p (Forward: 5’-CGCATGGCAGTGGTTTTACCCTA-3’; Reverse: 5’-ATCCAGTGCAGGGTCCGAGG-3’), and U6 small nuclear RNA (U6) (Forward: 5’-CGCTTCGGCAGCACATATACTAAAATTGGAAC-3’; Reverse: 5’-GCTTCACGAATTTGCGTGTCATCCTTGC-3’). The levels of circVPS33B, VPS33B, HNRNPK, and miR-873-5p were evaluated by $2^{-\Delta\Delta Ct}$ method, and β-actin or U6 was used as an internal.

Actinomycin D and RNase R treatment

The medium containing Actinomycin D (2 μg/mL, Sigma, St Louis, MO, USA) was utilized to inhibit RNA transcription of XGC-1 cells (0, 4, 8, 12, or 24 h). Total RNA of XGC-1 cells was incubated with 3 U/μg RNase R (Geneseed, Guangzhou, China) for total RNA digestion.

3-(4,5-dimethylthiazol-2-yl)-2,5-diphenyltetrazoliumbromide (MTT) assay

XGC-1 cells (5×10^3 cells) were seeded into 96-well plates and grown for different time (24 h, 48 h, or 72 h). After discarding the supernatant, MTT solution (100 μL, 0.5 mg/mL, Sigma) was supplemented into each well. After incubation for 4 h, the purple precipitate was dissolved with dimethylsulfoxide (DMSO) (150 μL, Sigma). Next, the Microplate Reader (Bio-Rad, Hercules, CA, USA) was utilized to evaluate the absorbance at 570 nm.

Plate clone assay

XGC-1 cells (5×10^3 cells/well) were seeded onto 6-well plates. 2 weeks later, XGC-1 cells were fixed by paraformaldehyde (4%, Sigma) and stained with crystal violet (0.5%, Sigma). Next, an inverted microscope (Nikon, Tokyo, Japan) was utilized to count and photograph the colonies (> 50 cells/colony).

Wound healing and transwell assays

The migration of XGC-1 cells was analyzed by wound healing and transwell assays. For wound healing assay, a wound on the cell layer was created using a pipette tip (100 μL) when the transfected XGC-1 cells reached 90% confluence. The pictures of the cells at 0 h and 24 h were photographed with an inverted microscope (Nikon). The migration rate was calculated according to the following equation: cell migration rate (%) = (1-the distance following healing/the distance prior to healing) ×100%.

For transwell migration assay, the serum-free containing transfected XGC-1 cells (1×10^5 cells) was added to the top chamber of the transwell chamber (8 μm, Costar, Cambridge, MA, USA). The cell medium containing 10% FBS was supplemented into the bottom of the transwell chamber. After removing the cells on the upper surface of the membrane, the remaining cells were fixed and stained with paraformaldehyde (4%, Sigma) and crystal violet (0.5%, Sigma), respectively. The migrating cells were calculated with an inverted microscope (Nikon) at 100 × magnification.

For transwell invasion assay, its method was the same as the cell migration assay. It was worth noting that the transwell chamber of the invasion assay was pre-coated with Matrigel (Sigma).

Western blotting

Total protein (tissue samples and cells) was separated using the RIPA lysis buffer (Solarbio). All antibodies were purchased from Santa Cruz Biotechnology (Santa Cruz, CA, USA). Western blotting was executed in light of the previous research [27]. The immunoblot was visualized through the enhanced chemiluminescence reagent kit (Beyotime, Shanghai, China). The primary antibodies including: anti-β-actin (sc-8432), anti-ki-67 (sc-23900), anti-E-cadherin (sc-21791), anti-N-cadherin (sc-59987), anti-vimentin (sc-373717), and anti-HNRNPK (sc-28380). Also, m-IgGκ BP-HRP (sc-516102) was used as the secondary antibody.

Analysis of extracellular acidification rate (ECAR) and oxygen consumption rate (OCR)

The XF96 Extracellular Flux analyzer (Seahorse Bioscience, Chicopee, MA, USA) was utilized for the assessment of the ECAR and OCR of transfected XGC-1 cells. In short, the cells (1×10^4) were seeded into a Seahorse XF 96 cell culture microplate. The Seahorse XF Glycolysis Stress Test Kit (Seahorse Bioscience) was applied for ECAR analysis. In short, glucose, oligomycin, and 2-deoxy-D-glucose (2-DG) were sequentially injected into each well at the specified time point after baseline measurement. The Seahorse XF Cell Mito Stress Test Kit (Seahorse Bioscience) was utilized for OCR evaluation. In brief, oligomycin, p-trifluoromethoxy carbonyl cyanide phenylhydrazone (FCCP), and rotenone (Rote) plus antimycin A (AA) were sequentially injected into each well after baseline measurement. At last, the data were analyzed with the Seahorse XF-96 Wave software, and ECAR and OCR were presented in mpH/min and pmoles/min, respectively.

Glycolysis assay

The supernatant of transfected XGC-1 cells was collected. The amount of lactate and glucose in the supernatant was assessed with a Glucose Assay kit (Sigma) or Lactate Assay kit (BioVision, Mountain View, CA, USA) in light of the manufacturer's instructions. Glucose uptake was analyzed by the difference between the glucose concentration and the control group.

Subcellular fractionation and localization

The nuclear RNA and cytoplasm RNA of XGC-1 cells were isolated by the PARIS kit (Life Technologies). Expression of circVPS33B in the nuclear and cytoplasm of XGC-1 cells was detected by qRT-PCR, and U6 and glyceraldehyde-3-phosphate dehydrogenase (GAPDH) were used as controls for nuclear and cytoplasm, respectively. The primers for GAPDH were as follows: (Forward: 5'-GACTCCACTCACGGCAAATTCA-3'; Reverse: 5'-TCGCTCCTGGAAGATGGTGAT-3')

Dual-luciferase reporter assay

The luciferase reporter assay kit (Promega, Madison, WI, USA) was employed to evaluate the luciferase activities of luciferase reporter vectors. The binding sites of circVPS33B in miR-873-5p were predicted with the circInteractome database. The binding sites between HNRNPK and miR-873-5p were predicted with the TarBase, TargetScan, miRDB, and miRWalk databases. The fragments of wild type (WT) circVPS33B (circVPS33B-WT), mutant (MUT) circVPS33B (circVPS33B-MUT), WT 3'UTR of HNRNPK (HNRNPK 3'UTR-WT), and MUT 3'UTR of HNRNPK (HNRNPK 3'UTR-MUT) containing miR-873-5p binding sites were synthesized and inserted into the psiCHECK-2 vectors (Promega), respectively, to construct the luciferase reporter vectors. After cotransfection of the luciferase reporter vectors with miR-873-5p or miR-NC into XGC-1 cells, the luciferase activities were evaluated by normalizing the firefly luminescence to Renilla luminescence.

RNA pull-down assay

The biotinylated (Bio)-miR-873-5p, Bio-miR-NC, and Bio-miR-873-5p-MUT probes were bought from Sigma. The probe-coated bead was established by incubating a probe with the M-280 Streptavidin magnetic bead (Invitrogen). The lysates of XGC-1 cells were incubated with probe-coated beads. The RNA complexes were isolated with TRIzol reagent (Solarbio). QRT-PCR was executed to analyze the enrichment level of circVPS33B in RNA complexes.

In vivo tumorigenesis assay

The protocols of xenograft assay were authorized by the Animal Ethics Committee of the Institute of Gastrointestinal Oncology, School of Medcine, Xiamen University. 10 BALB/c nude mice (4-week-old) were bought from Vital River Laboratory Animal Co., Ltd. (Beijing, China). For xenograft assay, XGC-1 cells (1×10^6) with sh-circVPS33B or sh-NC were subcutaneously injected into the right flank of BALB/c nude mice. Tumor volume was measured with calipers every 7 days from the second week after injection. Until day 35, the mice were killed by cervical dislocation under isoflurane (5%) to take tumor tissues. Tumors volume was counted in light of the following equation: Volume = (length $\times$width^2)/2. The mice were randomly divided into 2 groups with five mice per group.

Statistical analysis

Correlation among circVPS33B, HNRNPK, and miR-873-5p in infiltrative GC tissues were evaluated with the Pearson's correlation analysis. Differences were deemed significant if $P < 0.05$. One-way variance analysis (ANOVA) with Turkey's post hoc test was utilized to assess the differences among 3 or more groups. Paired or unpaired Student's *t* test was applied to compare the difference between 2 groups. Statistical analysis was implemented with GraphPad Prism 6 software (GraphPad, San Diego, CA, USA). The experiments *in vitro* were repeated at least 3 times, and data were exhibited as the mean ± standard deviation.

Results

Expression and characteristics of circVPS33B in infiltrative GC

In the research, we first searched the public database (GES78092) and noted that there were 199 differentially expression circRNAs in GC tissues (Fig. 1A). Among the differentially expression circRNAs, we selected the top 10 upregulated and 10 downregulated differentially expression circRNAs to draw a heat map, as exhibited in Fig. 1B. Moreover, we selected circVPS33B (hsa_circ_0005529) as the target for further investigation. CircVPS33B is a 193 bp transcript derived from the VPS33B gene (Fig. 1C). Next, we detected the expression of circVPS33B in 37 paired infiltrative GC tissues and neighboring non-tumor tissues. QRT-PCR results also displayed that circVPS33B expression was elevated in infiltrative GC tissues in contrast to the neighboring non-tumor tissues (Fig. 1D). Also, circVPS33B expression was increased in XGC-1 cells compared to the GES-1 cells (Fig. 1E). We also explored the characteristics of circVPS33B in XGC-1 cells. Actinomycin D assay revealed that circVPS33B was more stable than linear VPS33B in XGC-1 cells, implying that circVPS33B can be a suitable prognosis and diagnostic marker (Fig. 1F). RNase R digestion assay presented that circVPS33B was resistant to RNase R, whereas the linear VPS33B was degraded by RNase R treatment (Fig. 1G). These data indicated that high circVPS33B expression might be associated with the development of infiltrative GC.

Inhibition of circVPS33B reduced the malignancy and Warburg effect of infiltrative GC cells

Subsequently, we investigated the biological role of circVPS33B in infiltrative GC via loss-of-function assays. We designed the siRNA targeting circVPS33B and transfected into XGC-1 cells. Compared to the control si-NC, circVPS33B expression was apparently reduced in XGC-1 cells after si-circVPS33B transfection (Fig. 2A). MTT assay exhibited that reduced circVPS33B expression inhibited cell proliferation in XGC-1 cells relative to the control group (Fig. 2B). Plate clone assay displayed that circVPS33B silencing decreased the colony formation number of XGC-1 cells (Fig. 2C). Wound healing assay showed that the migration of XGC-1 cells was repressed by circVPS33B knockdown (Fig. 2D). Transwell assay indicated that circVPS33B knockdown played an inhibitory effect on the migration and invasion of XGC-1 cells (Fig. 2E and 2F). Results of western blotting showed that the levels of ki-67, N-cadherin, and Vimentin were downregulated in circVPS33B-silenced XGC-1 cells, while the level of E-cadherin was upregulated (Fig. 2G). Moreover, we also analyzed the ECAR and OCR of XGC-1 cells with an XF96 extracellular flux analyzer. The results exhibited silenced circVPS33B expression decreased the ECAR of XGC-1 cells and increased the OCR of XGC-1 cells (Fig. 2H and 2I). Furthermore, glycolysis assay presented that downregulation of circVPS33B could reduce glucose uptake and lactate production in XGC-1 cells (Fig. 2J and 2K). Taken together, these data indicated that circVPS33B knockdown could decrease cell malignant behaviors and Warburg effect in infiltrative GC cells.

CircVPS33B was identified as a sponge for miR-873-5p in infiltrative GC cells

In consideration of the above findings, we further explored the latent regulatory mechanism of circVPS33B in infiltrative GC. We first explored the subcellular localization of circVPS33B in XGC-1 cells. QRT-PCR presented that circVPS33B was mainly distributed in the cytoplasmic fraction of XGC-1 cells, indicating that circVPS33B had potential post-transcriptional regulation (Fig. 3A). Moreover, we

discovered that miR-873-5p possessed complementary binding sites for circVPS33B through circInteractome database (Fig. 3B). In addition, to analyze the efficiency of miR-873-5p overexpression in XGC-1 cells, qRT-PCR was utilized to measure the level of miR-873-5p. And result showed that the expression level of miR-873-5p was markedly up-regulated after transfection with miR-873-5p (Fig. 3C). Dual-luciferase reporter assay indicated that miR-873-5p overexpression could reduce the luciferase intensity of luciferase reporters with circVPS33B-WT in XGC-1 cells, whereas the luciferase intensity of luciferase reporters with circVPS33B-MUT did not affect (Fig. 3D). RNA pull-down assay presented that circVPS33B could be pulled down by Bio-miR-873-5p probe relative to the Bio-miR-NC and Bio-miR-873-5p-MUT probes (Fig. 3E). Moreover, the public database (GES78091) showed that miR-873-5p was downregulated in GC tissues (Fig. 3F). Also, we observed that miR-873-5p expression was decreased in infiltrative GC tissues compared to the neighboring non-tumor tissues (Fig. 3G). Likewise, miR-873-5p was downregulated in XGC-1 cells than that in GES-1 cells (Fig. 3H). Pearson's correlation analysis indicated that miR-873-5p and circVPS33B had a negative correlation in infiltrative GC tissues (Fig. 3I). Furthermore, decreased circVPS33B expression could elevate miR-873-5p expression in XGC-1 cells (Fig. 3J). However, miR-873-5p mimic had no effect on the level of circVPS33B in XGC-1 cells (Fig. 3K). Collectively, these findings manifested that circVPS33B acted as a sponge for miR-873-5p in infiltrative GC cells.

MiR-873-5p inhibition reversed circVPS33B silencing-mediated effects on the malignancy and Warburg effect of infiltrative GC cells

Given that circVPS33B acted as a sponge for miR-873-5p in XGC-1 cells, we further explored whether miR-873-5p was connected with circVPS33B-mediated infiltrative GC progression. We discovered that miR-873-5p inhibitor reversed the upregulation of miR-873-5p in XGC-1 cells caused by circVPS33B knockdown (Fig. 4A). Moreover, reduced miR-873-5p expression overturned the inhibitory impact of circVPS33B silencing on the proliferation, colony formation, migration, and invasion of XGC-1 cells (Fig. 4B-4F). Moreover, both the upregulation of E-cadherin and the downregulation of ki-67, N-cadherin, and Vimentin in XGC-1 cells caused by circVPS33B inhibition were restored by miR-873-5p knockdown (Fig. 4G). Furthermore, silenced miR-873-5p expression abolished the decrease of ECAR and the elevation of OCR in circVPS33B-inhibited XGC-1 cells (Fig. 4H and 4I). Also, the repressive effect of circVPS33B knockdown on glucose uptake and lactate production of XGC-1 cells was overturned by reducing miR-873-5p expression (Fig. 4J and 4K). Overall, these findings manifested that circVPS33B modulated the malignancy and Warburg effect of infiltrative GC cells via sponging miR-873-5p.

CircVPS33B could regulate HNRNPK expression through competitively binding to miR-873-5p

Next, we further investigated whether circVPS33B could regulate the target of miR-873-5p via competitively binding to miR-873-5p through acting as a competing endogenous RNA (ceRNA). We predicted the target of miR-873-5p through cross-analyzing four prediction databases: TarBase, TargetScan, miRDB, and miRWalk. As shown in Fig. 5A, there were 13 genes with complementary binding sites for miR-873-5p. Based on the pre-experiment, we chose HNRNPK for further research. The

complementary binding sites between miR-873-5p and HNRNPK were displayed in Fig. 5B. Moreover, dual-luciferase reporter assay revealed that elevated miR-873-5p expression reduced the luciferase activity of the luciferase reporters containing HNRNPK 3'UTR-WT in XGC-1 cells, but there was no overt difference in the luciferase reporters containing HNRNPK 3'UTR-MUT (Fig. 5C). We also observed that HNRNPK mRNA and protein levels were elevated in infiltrative GC tissues compared to the neighboring non-tumor tissues (Fig. 5D and 5E). Consistently, HNRNPK mRNA and protein levels were also increased in XGC-1 cells (Fig. 5F and 5G). Moreover, the expression of HNRNPK mRNA in infiltrative GC tissues had a negative correlation with miR-873-5p (Fig. 5H). Furthermore, miR-873-5p mimic reduced the levels of HNRNPK mRNA and protein in XGC-1 cells, while this decrease was reversed by transfection of pcDNA-HNRNPK (Fig. 5I and 5J). Also, HNRNPK mRNA expression was positively correlated with circVPS33B in infiltrative GC tissues (Fig. 5K). Downregulation of circVPS33B could reduce the levels of HNRNPK mRNA and protein in XGC-1 cells, but this trend was overturned by miR-873-5p inhibition (Fig. 5L and 5M). Collectively, these results manifested that circVPS33B regulated HNRNPK expression via sponging miR-873-5p in infiltrative GC cells.

HNRNPK overexpression abolished miR-873-5p mimic-mediated effects on the malignancy and Warburg effect of infiltrative GC cells

We further investigated whether miR-873-5p regulated the malignancy and Warburg effect of XGC-1 cells via targeting HNRNPK. The results exhibited that the repressive impact of miR-873-5p mimic on cell proliferation, colony formation, migration, and invasion in XGC-1 cells was reversed by HNRNPK elevation (Fig. 6A-6E). Moreover, miR-873-5p overexpression reduced ki-67, N-cadherin, and Vimentin levels and increased E-cadherin level in XGC-1 cells, but these impacts were overturned by forcing HNRNPK expression (Fig. 6F). Additionally, forced miR-873-5p expression decreased ECAR and elevated OCR of XGC-1 cells, but these tendencies were abolished after HNRNPK overexpression (Fig. 6G and 6H). Furthermore, elevated HNRNPK expression restored the decrease of glucose uptake and lactate production in XGC-1 cells mediated by miR-873-5p upregulation (Fig. 6I and 6J). Overall, these data indicated that miR-873-5p regulated the malignancy and Warburg effect of infiltrative GC cells via targeting HNRNPK.

Silence of circVPS33B reduced tumor growth *in vivo*

To verify the role of circVPS33B on tumor growth *in vivo*, we injected XGC-1 cells stably transfected with sh-circVPS33B or sh-NC into BALB/c nude mice. The results presented that tumor volume and weight were signally reduced in the circVPS33B silencing group in contrast to the control group (Fig. 7A and 7B). QRT-PCR revealed that circVPS33B and HNRNPK protein were overtly downregulated in mice tumor tissues of the circVPS33B silencing group, but miR-873-5p expression was apparently increased (Fig. 7C-7E). Together, these data manifested that circVPS33B inhibition could decrease tumor growth *in vivo*.

Discussion

Mounting studies have indicated that circRNAs are promising biomarkers and targets for disease diagnosis and treatment [28, 29]. In the research, we explored the role and regulatory mechanism of circVPS33B in infiltrative GC development.

Increasing evidence proved that circRNAs were connected with the advancement of GC. For instance, circRNA circ_MAT2B contributed to cell growth and glycolysis through sponging miR-515-5p and upregulating HIF-1α in GC [30]. Similarly, circRNA circ_CCDC9 inhibited GC progression via modulating CAV1 expression through sponging miR-6792-3p [31]. In the current work, circVPS33B was upregulated in infiltrative GC tissues and cells. Silence of circVPS33B reduced tumor growth *in vivo* and repressed the malignancy and Warburg effect of infiltrative GC cells *in vitro*. Warburg effect, also known as aerobic glycolysis, accelerates cancer cell growth through elevating glucose uptake and lactate production [32]. Wang *et al*. uncovered that circRNA circ_FOXP1 accelerated the Warburg effect and tumor growth in gallbladder cancer [33]. Therefore, these data manifested that circVPS33B knockdown could reduce tumor growth and Warburg effect in infiltrative GC.

Studies have disclosed that some circRNAs can be used as ceRNAs to modulate the expression of some genes and thus participate in the advancement of certain tumors [10, 30, 31]. In this study, we discovered circVPS33B served as a sponge for miR-873-5p. MiR-873-5p was revealed to be implicated in certain tumors progression. Zhu *et al*. uncovered that miR-873-5p could curb colon cancer progression via repressing the TUSC3/AKT pathway [34]. Another research disclosed that miR-873-5p reduced cell invasion and migration through targeting CXCL16 in papillary thyroid cancer [18]. In GC, miR-873-5p expression could be inhibited by lncRNA TDRG1 or lncRNA DDX11-AS1, thereby accelerating the aggressiveness of GC [20, 21]. Herein, miR-873-5p expression had a negative correlation with circVPS33B in infiltrative GC tissues. Downregulation of miR-873-5p reversed the repressive impact of circVPS33B downregulation on the malignancy and Warburg effect of infiltrative GC cells. Therefore, we inferred that circVPS33B regulated infiltrative GC progression and Warburg effect via miR-873-5p.

HNRNPK, an oncogene, is involved in the development of tumors. One report revealed that lncRNA pancEts-1 could facilitate neuroblastoma progression by HNRNPK-mediated the stabilization of β-Catenin [35]. Xu *et al*. proved that HNRNPK promoted cell colony formation and proliferation in lung adenocarcinoma cells [36]. Peng *et al*. reported that HNRNPK contributed to cell invasion, migration, and proliferation via regulation of the alternative splicing of CD44E in GC cells [26]. In our work, we discovered that HNRNPK was a target of miR-873-5p. Moreover, miR-873-5p regulated infiltrative GC cell malignant behaviors and Warburg effect via HNRNPK. Also, circVPS33B could modulate HNRNPK expression via competitively binding to miR-873-5p. Overall, we concluded that circVPS33B regulated infiltrative GC malignant behaviors and Warburg effect via sponging miR-873-5p and regulating HNRNPK expression.

Conclusion

In sum, circVPS33B played an accelerative role in infiltrative GC progression. Moreover, circVPS33B downregulation reduced infiltrative GC advancement and Warburg effect through modulating HNRNPK

expression through sponging miR-873-5p, manifesting that circVPS33B might be a hopeful target for infiltrative GC treatment.

Declarations

Acknowledgements

Not applicable.

Funding:

This work was supported by grant from The National Natural Science Foundation of China(Nos. 81871979 and 81372616); Fujian Provincial Medical Innovation Project (No. 2017-CXB-15); Guiding Project of Xiamen Science and Technology Plan（3502Z20149005 3502Z20174076）; Young and Middle-aged Backbone Key Research Project of National Health and Family Planning Commission of Fujian Province(2017-ZQN-89)

Availability of data and materials

The analyzed data sets generated during the present study are available from the corresponding author on reasonable request.

Ethics approval and consent to participate

The present study was approved by the ethical review committee of The Second Hospital of Hebei Medical University. Written informed consent was obtained from all enrolled patients.

Patient consent for publication

Not applicable.

Competing interests

The authors declare that they have no competing interests.

References

1. Bray F, et al. Global cancer statistics 2018: GLOBOCAN estimates of incidence and mortality worldwide for 36 cancers in 185 countries. Cancer J Clin. 2018;68(6):394–424.
2. Piard F, et al. [Does Ming's classification of gastric carcinomas have epidemiologic or prognostic value?]. Annales de pathologie. 1986;6(4–5):329–34.
3. Luebke T, et al. Histological grading in gastric cancer by Ming classification: correlation with histopathological subtypes, metastasis, and prognosis. World journal of surgery 2005;29(11).

4. Kanda M, et al. Tumor Infiltrative Pattern Predicts Sites of Recurrence After Curative Gastrectomy for Stages 2 and 3 Gastric Cancer. Ann Surg Oncol. 2016;23(6):1934–40.
5. Nakagawa N, et al. Pathological tumor infiltrative pattern and sites of initial recurrence in stage II/III gastric cancer: Propensity score matching analysis of a multi-institutional dataset. Cancer medicine. 2018;7(12):6020–9.
6. Li X, et al. The Biogenesis, Functions, and Challenges of Circular RNAs. Molecular cell. 2018;71(3):428–42.
7. Li H-M, et al. Intriguing circles: Conflicts and controversies in circular RNA research. Wiley interdisciplinary reviews RNA. 2019;10(5):e1538.
8. Zhao W, et al. Circular RNAs: A novel target among non–coding RNAs with potential roles in malignant tumors (Review). Mol Med Rep. 2019;20(4):3463–74.
9. Wang Y, et al. Exosomal circRNAs: biogenesis, effect and application in human diseases. Mol Cancer. 2019;18(1):116.
10. Wang Y, et al. Circular RNA hsa_circ_0003141 promotes tumorigenesis of hepatocellular carcinoma via a miR-1827/UBAP2 axis. Aging 2020;12(.
11. Huang Y-S, et al. Expression profile of circular RNAs in human gastric cancer tissues. Mol Med Rep. 2017;16(3):2469–76.
12. Lu TX, et al. MicroRNA The Journal of allergy clinical immunology. 2018;141(4):1202–7.
13. Saliminejad K, et al. An overview of microRNAs: Biology, functions, therapeutics, and analysis methods. Journal of cellular physiology. 2019;234(5):5451–65.
14. Rupaimoole R, et al. MicroRNA therapeutics: towards a new era for the management of cancer and other diseases. Nature reviews Drug discovery. 2017;16(3):203–22.
15. Zhang L, et al. MicroRNA-34 family: a potential tumor suppressor and therapeutic candidate in cancer. Journal of experimental clinical cancer research: CR. 2019;38(1):53.
16. Fernández-Ramos D, et al. MiR-873-5p acts as an epigenetic regulator in early stages of liver fibrosis and cirrhosis. Cell death disease. 2018;9(10):958.
17. Lin YH, et al. Long non-coding RNA HOTAIRM1 promotes proliferation and inhibits apoptosis of glioma cells by regulating the miR-873-5p/ZEB2 axis. Chin Med J (Engl). 2020;133(2):174–82.
18. Wang Z, et al. miR-873-5p Inhibits Cell Migration and Invasion of Papillary Thyroid Cancer via Regulation of CXCL16. Onco Targets Ther. 2020;13:1037–46.
19. Wang L, et al. MiR-873-5p suppresses cell proliferation and epithelial-mesenchymal transition via directly targeting Jumonji domain-containing protein 8 through the NF-κB pathway in colorectal cancer. J Cell Commun Signal. 2019;13(4):549–60.
20. Ma Y, et al. LncRNA TDRG1 promotes the aggressiveness of gastric carcinoma through regulating miR-873-5p/HDGF axis. Biomed Pharmacother. 2020;121:109425.
21. Ren Z, et al. Long non-coding RNA DDX11-AS1 facilitates gastric cancer progression by regulating miR-873-5p/SPC18 axis. Artif Cells Nanomed Biotechnol. 2020;48(1):572–83.

22. Wang Z, et al. The emerging roles of hnRNPK. Journal of cellular physiology. 2020;235(3):1995–2008.
23. Wiesmann N, et al. Knockdown of hnRNPK leads to increased DNA damage after irradiation and reduces survival of tumor cells. Carcinogenesis. 2017;38(3):321–8.
24. Chen X, et al. Heterogeneous nuclear ribonucleoprotein K is associated with poor prognosis and regulates proliferation and apoptosis in bladder cancer. J Cell Mol Med. 2017;21(7):1266–79.
25. Gao T, et al. Exosomal lncRNA 91H is associated with poor development in colorectal cancer by modifying HNRNPK expression. Cancer Cell Int. 2018;18:11.
26. Peng W-Z, et al. hnRNPK promotes gastric tumorigenesis through regulating CD44E alternative splicing. Cancer cell international. 2019;19:335.
27. Zhou M, et al. Overexpression of the long non-coding RNA SPRY4-IT1 promotes tumor cell proliferation and invasion by activating EZH2 in hepatocellular carcinoma. Biomedicine & pharmacotherapy = Biomedecine & pharmacotherapie 2017;85(348 – 54.
28. Chen X, et al. Circular RNAs in immune responses and immune diseases. Theranostics. 2019;9(2):588–607.
29. Lei B, et al. Circular RNA: a novel biomarker and therapeutic target for human cancers. International journal of medical sciences. 2019;16(2):292–301.
30. Liu J, et al. Circular RNA circ-MAT2B facilitates glycolysis and growth of gastric cancer through regulating the miR-515-5p/HIF-1α axis. Cancer cell international. 2020;20:171.
31. Luo Z, et al. Circular RNA circCCDC9 acts as a miR-6792-3p sponge to suppress the progression of gastric cancer through regulating CAV1 expression. Mol Cancer. 2020;19(1):86.
32. Liberti MV, et al. The Warburg Effect: How Does it Benefit Cancer Cells? Trends Biochem Sci. 2016;41(3):211–8.
33. Wang S, et al. Circular RNA FOXP1 promotes tumor progression and Warburg effect in gallbladder cancer by regulating PKLR expression. Mol Cancer. 2019;18(1):145.
34. Zhu Y, et al. miR-873-5p inhibits the progression of colon cancer via repression of tumor suppressor candidate 3/AKT signaling. Journal of gastroenterology hepatology. 2019;34(12):2126–34.
35. Li D, et al. Long Noncoding RNA pancEts-1 Promotes Neuroblastoma Progression through hnRNPK-Mediated β-Catenin Stabilization. Cancer research. 2018;78(5):1169–83.
36. Xu L, et al. YAP mediates the positive regulation of hnRNPK on the lung adenocarcinoma H1299 cell growth. Acta Biochim Biophys Sin. 2019;51(7):677–87.

Figures

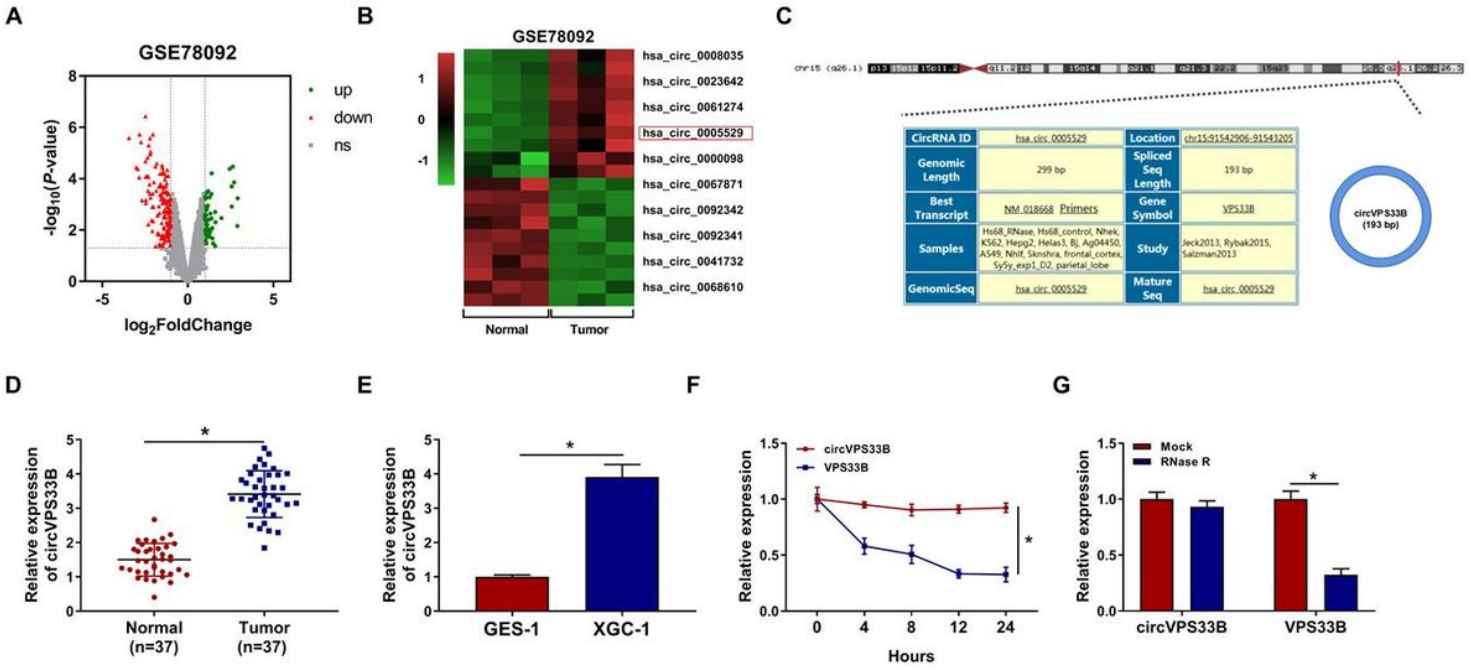

Figure 1

CircVPS33B was upregulated in infiltrative GC tissues and cells. (A) The volcano plot showed differentially expressed circRNAs in GC tissues (GES78092). Green represented upregulated circRNAs and red represented downregulated circRNAs. (B) Heatmap exhibited the top 10 upregulated and 10 downregulated differentially expression circRNAs in GC tissues (GES78092). (C) Schematic diagram illustrated the formation of circVPS33B originated from the VPS33B pre-mRNA. (D and E) QRT-PCR displayed the expression of circVPS33B in 37 paired infiltrative GC tissues and neighboring non-tumor tissues, as well as XGC-1 and GES-1 cells. (F and G) After Actinomycin D or RNase R treatment, the levels of circVPS33B and VPS33B mRNA were analyzed by qRT-PCR. *P < 0.05.

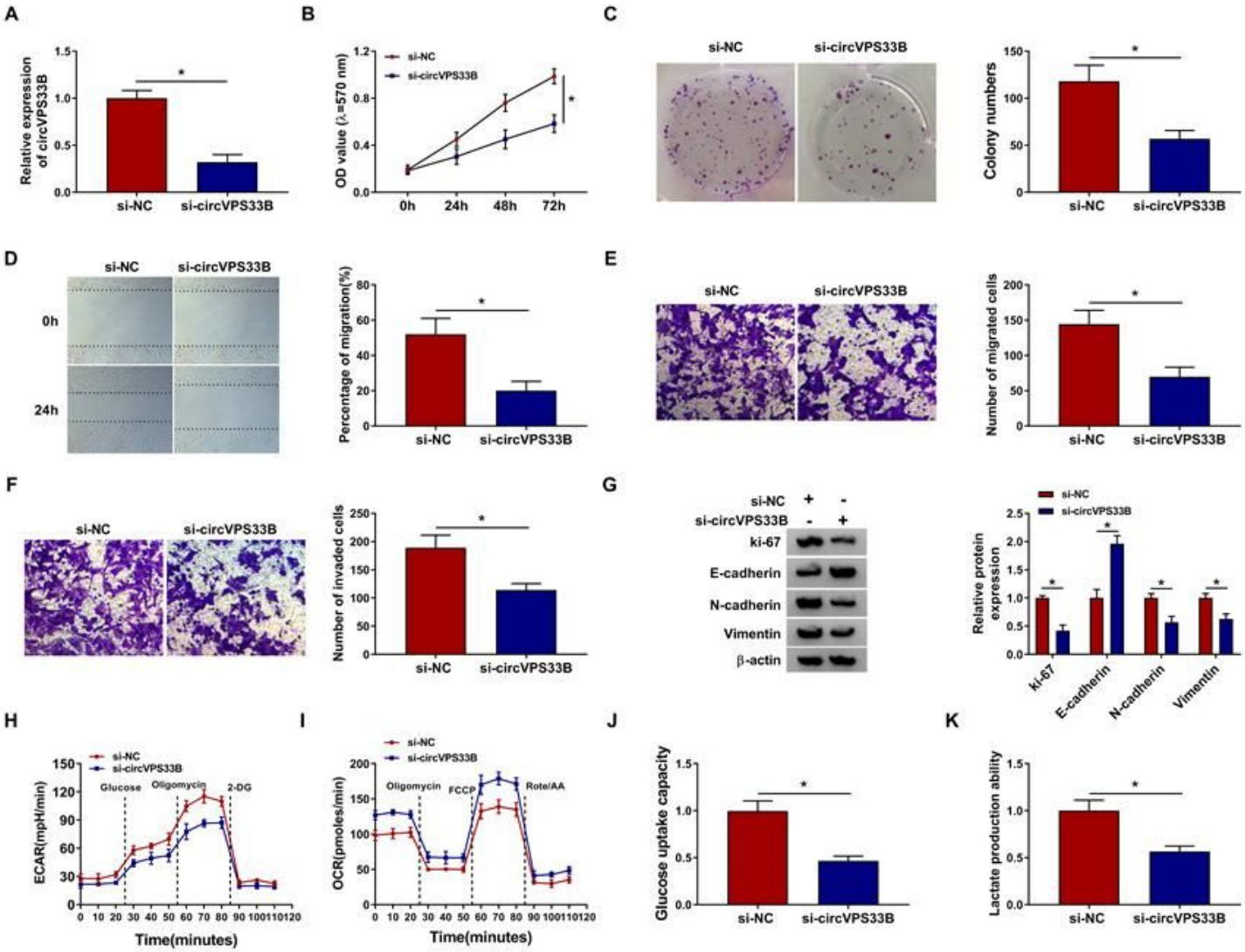

Figure 2

Impacts of circVPS33B inhibition on the malignancy and Warburg effect of infiltrative GC cells. (A) The transfection efficiency of XGC-1 cells was analyzed with qRT-PCR. (B-F) The proliferation, colony formation, migration, and invasion of XGC-1 cells transfected with si-NC or si-circVPS33B were analyzed via MTT, plate clone, wound healing, or transwell assays. (G) After si-NC or si-circVPS33B transfection, the levels of ki-67, E-cadherin N-cadherin, and Vimentin in XGC-1 were examined by western blotting. (H and I) An XF96 extracellular flux analyzer was employed to analyze the ECAR and OCR of XGC-1 cells transfected with si-NC or si-circVPS33B. (J and K) Glycolysis assay was performed to evaluate glucose uptake and lactate production in XGC-1 cells transfected with si-NC or si-circVPS33B. *P < 0.05.

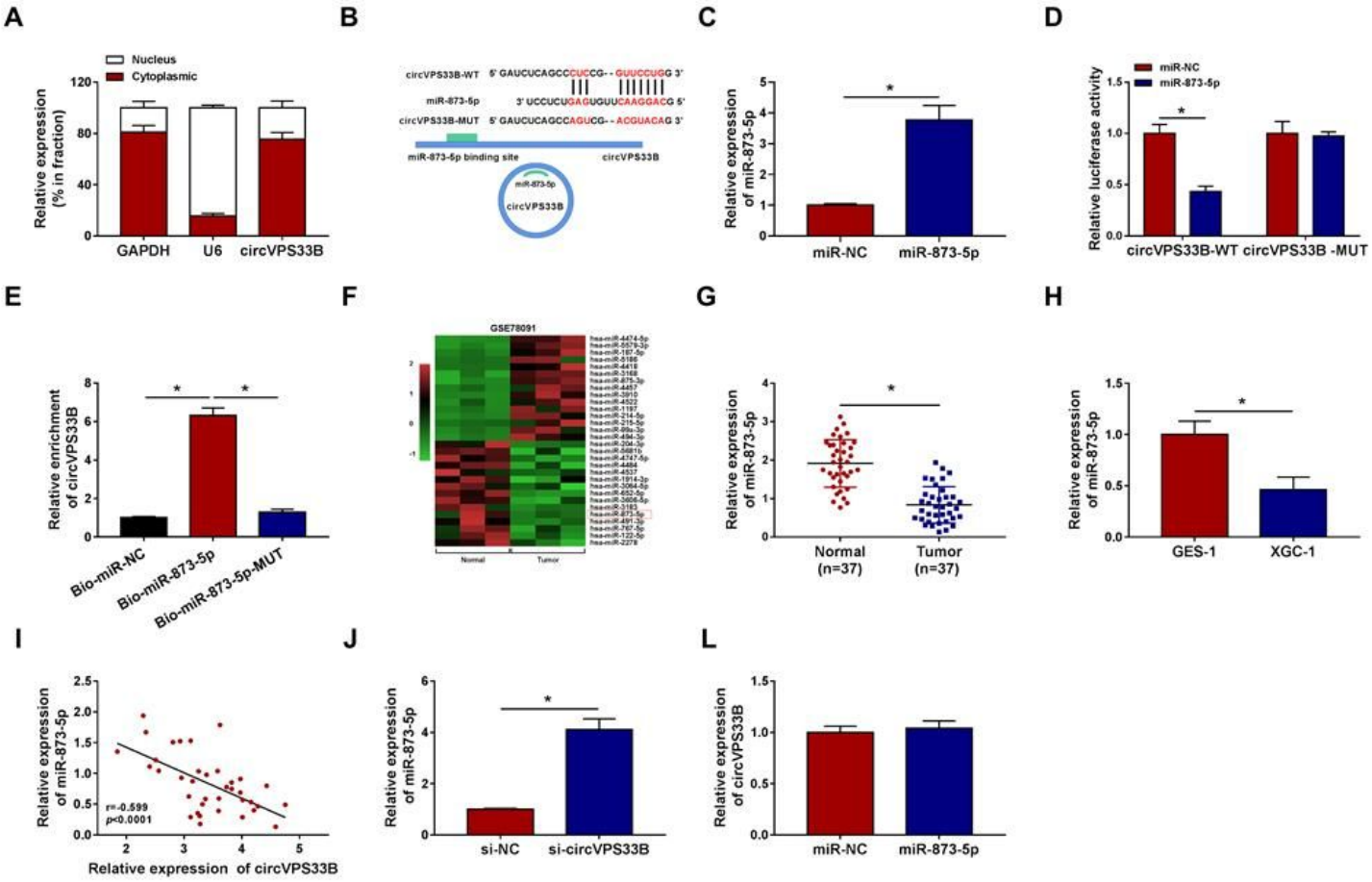

Figure 3

CircVPS33B served as a sponge for miR-873-5p in infiltrative GC cells. (A) The subcellular localization of circVPS33B in XGC-1 cells was analyzed by qRT-PCR. (B) Schematic diagram displayed the binding sites between circVPS33B and miR-873-5p. (C) The expression level of miR-873-5p was measured by qRT-PCR. (D) Dual-luciferase reporter assay was executed to assess the possible binding sites between circVPS33B and miR-873-5p. (E) After RNA pull-down assay, the level of circVPS33B was measured with qRT-PCR. (F) Heatmap exhibited the differentially expression miRs in GC tissues (GES78091). (G and H) Expression of miR-873-5p in 37 paired infiltrative GC tissues and neighboring non-tumor tissues, as well as XGC-1 and GES-1 cells was analyzed by qRT-PCR. (I) The correlation between circVPS33B and miR-873-5p was analyzed by Pearson's correlation analysis. (J) Influence of circVPS33B silencing on the expression of miR-873-5p was determined by qRT-PCR. (K) Impact of miR-873-5p elevation on the level of circVPS33B was evaluated with qRT-PCR. *P < 0.05.

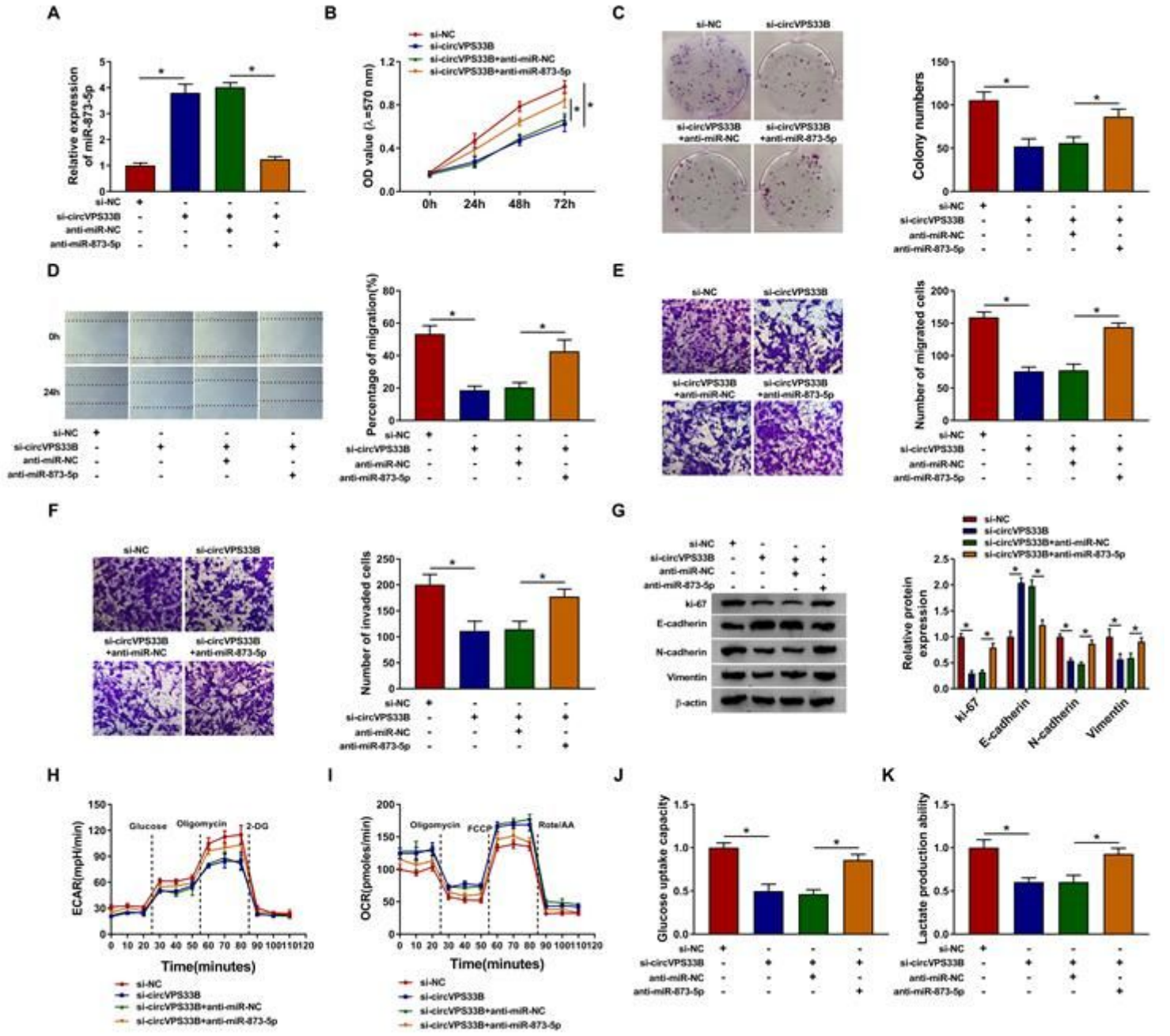

Figure 4

CircVPS33B played its role through sponging miR-873-5p. (A-K) XGC-1 cells were transfected with si-NC, si-circVPS33B, si-circVPS33B+anti-miR-NC, or si-circVPS33B+anti-miR-873-5p. (A) QRT-PCR was executed to analyze the level of miR-873-5p in XGC-1 cells. (B-F) MTT, plate clone, wound healing, and transwell assays were employed to evaluate the proliferation, colony formation, migration, or invasion capacity of XGC-1 cells. (G) Western blotting was conducted to detect the levels of ki-67, E-cadherin, N-cadherin, and Vimentin in XGC-1 cells. (H and I) The ECAR and OCR of XGC-1 cells were analyzed by XF96 extracellular flux analyzer. (J and K) Glucose uptake and lactate production in XGC-1 cells were assessed by glycolysis assay. *P < 0.05.

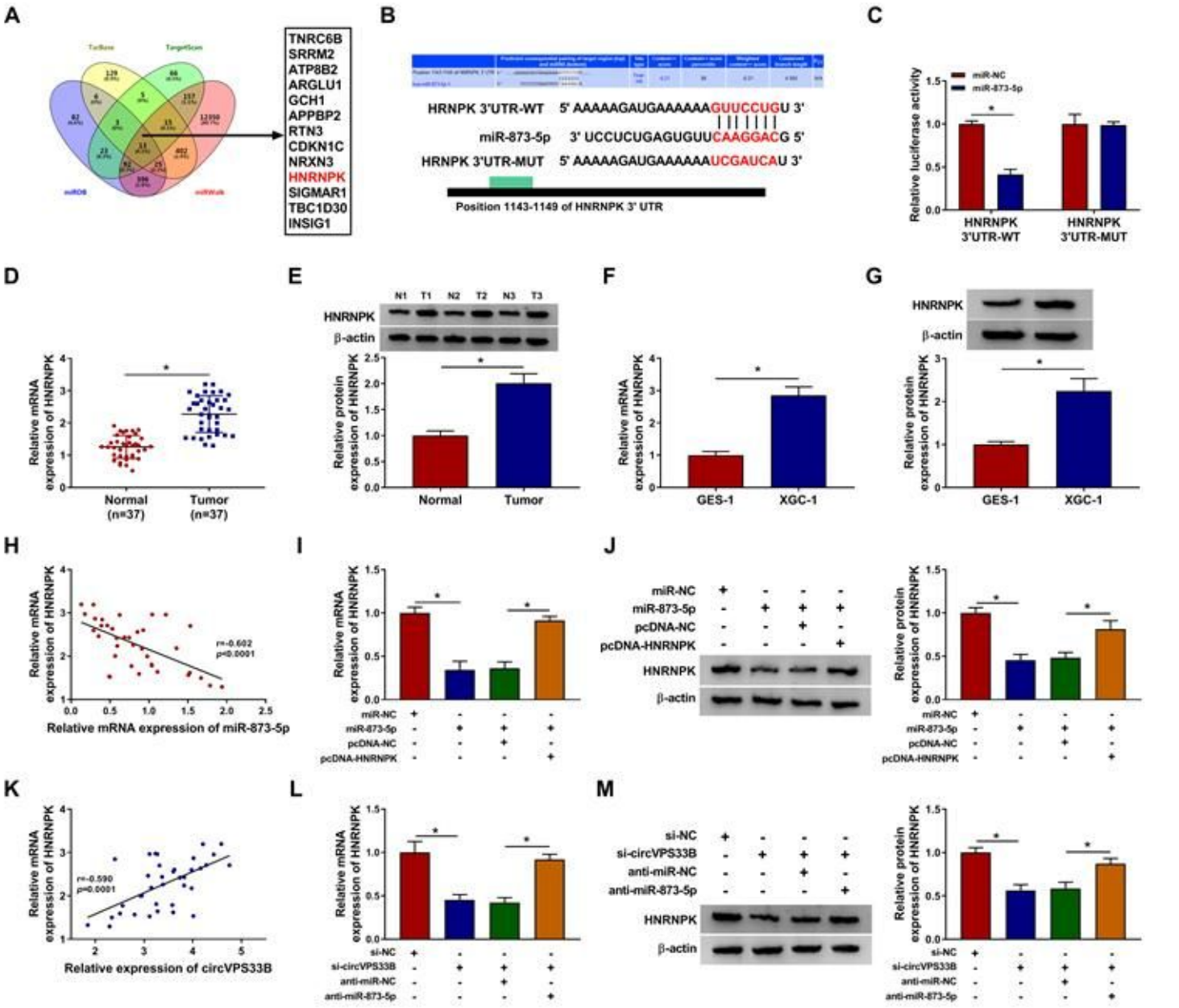

Figure 5

HNRNPK expression could be regulated by the circVPS33B/miR-873-5p axis. (A) The targets of miR-873-5p were predicted by cross-analyzing four prediction databases: TarBase, TargetScan, miRDB, and miRWalk. (B) Schematic diagram displayed showed the putative binding sites of HNRNPK associated with miR-873-5p. (C) Dual-luciferase reporter assay verified the possible binding sites between miR-873-5p and HNRNPK. (D-G) The levels of HNRNPK mRNA and protein in infiltrative GC tissues and neighboring non-tumor tissues, as well as XGC-1 and GES-1 cells were measured by qRT-PCR or western blotting. (H) Pearson's correlation analysis exhibited the correlation between miR-873-5p and HNRNPK in infiltrative GC tissues. (I and J) The levels of HNRNPK mRNA and protein in XGC-1 cells transfected with miR-NC, miR-873-5p, miR-873-5p+pcDNA-NC, or miR-873-5p+pcDNA-HNRNPK were examined using qRT-PCR or western blotting. (K) Pearson's correlation analysis revealed the correlation between circVPS33B

and HNRNPK in infiltrative GC tissues. (L and M) The mRNA and protein levels of HNRNPK in XGC-1 cells transfected with si-NC, si-circVPS33B, si-circVPS33B+anti-miR-NC, or si-circVPS33B+anti-miR-873-5p were analyzed using qRT-PCR or western blotting. *P < 0.05.

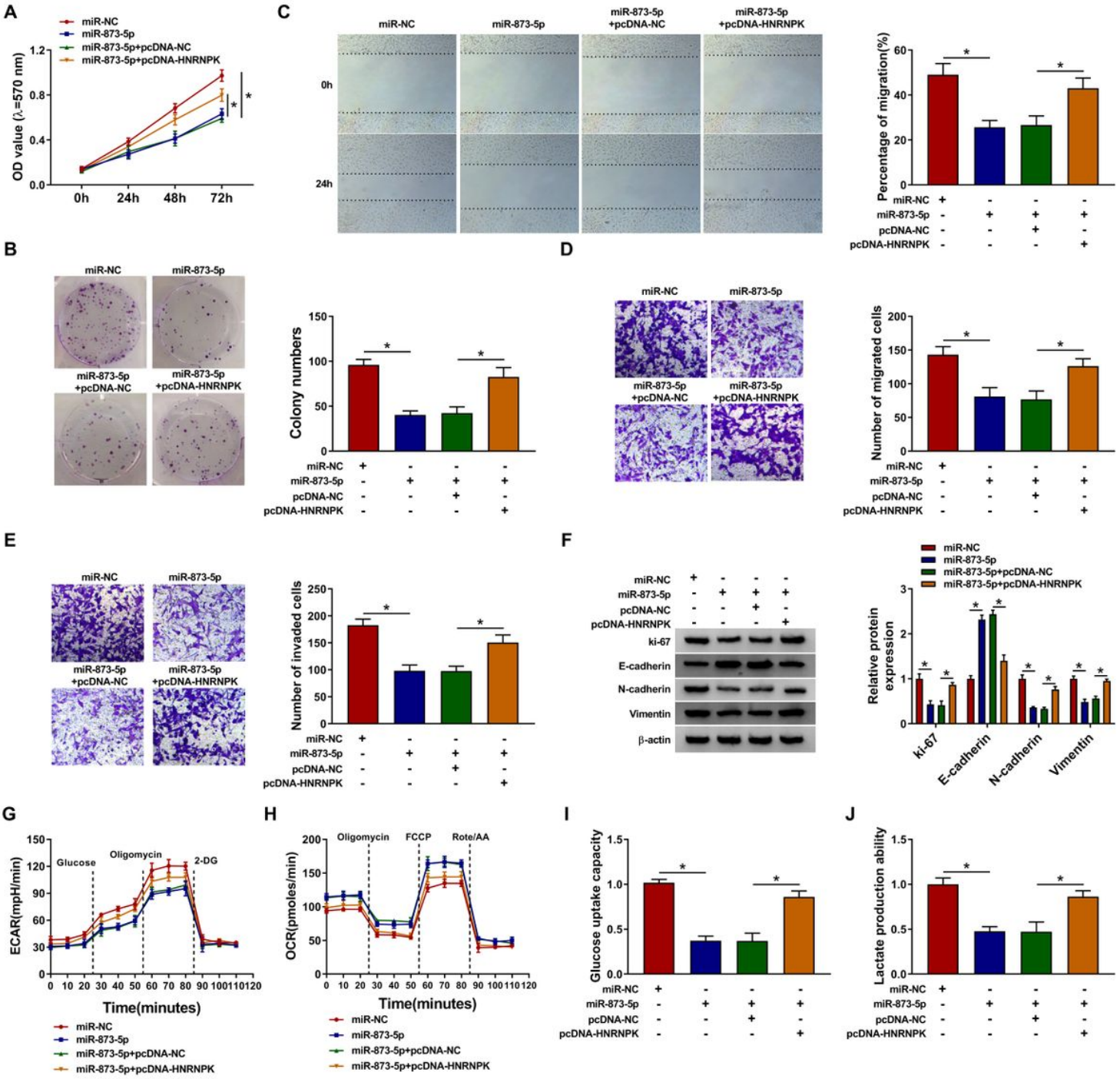

Figure 6

MiR-873-5p exerted its role via targeting HNRNPK. (A-J) XGC-1 cells were transfected with miR-NC, miR-873-5p, miR-873-5p+pcDNA-NC, or miR-873-5p+pcDNA-HNRNPK. (A-E) The proliferation, colony formation, migration, and invasion capacities of XGC-1 cells were analyzed by MTT, plate clone, wound healing, or transwell assays. (F) Western blotting revealed the levels of ki-67, E-cadherin, N-cadherin, and

Vimentin in XGC-1 cells. (G and H) The ECAR and OCR of XGC-1 cells were assessed with an XF96 extracellular flux analyzer. (I and J) Glycolysis assay analyzed glucose uptake and lactate production in XGC-1 cells. *P < 0.05.

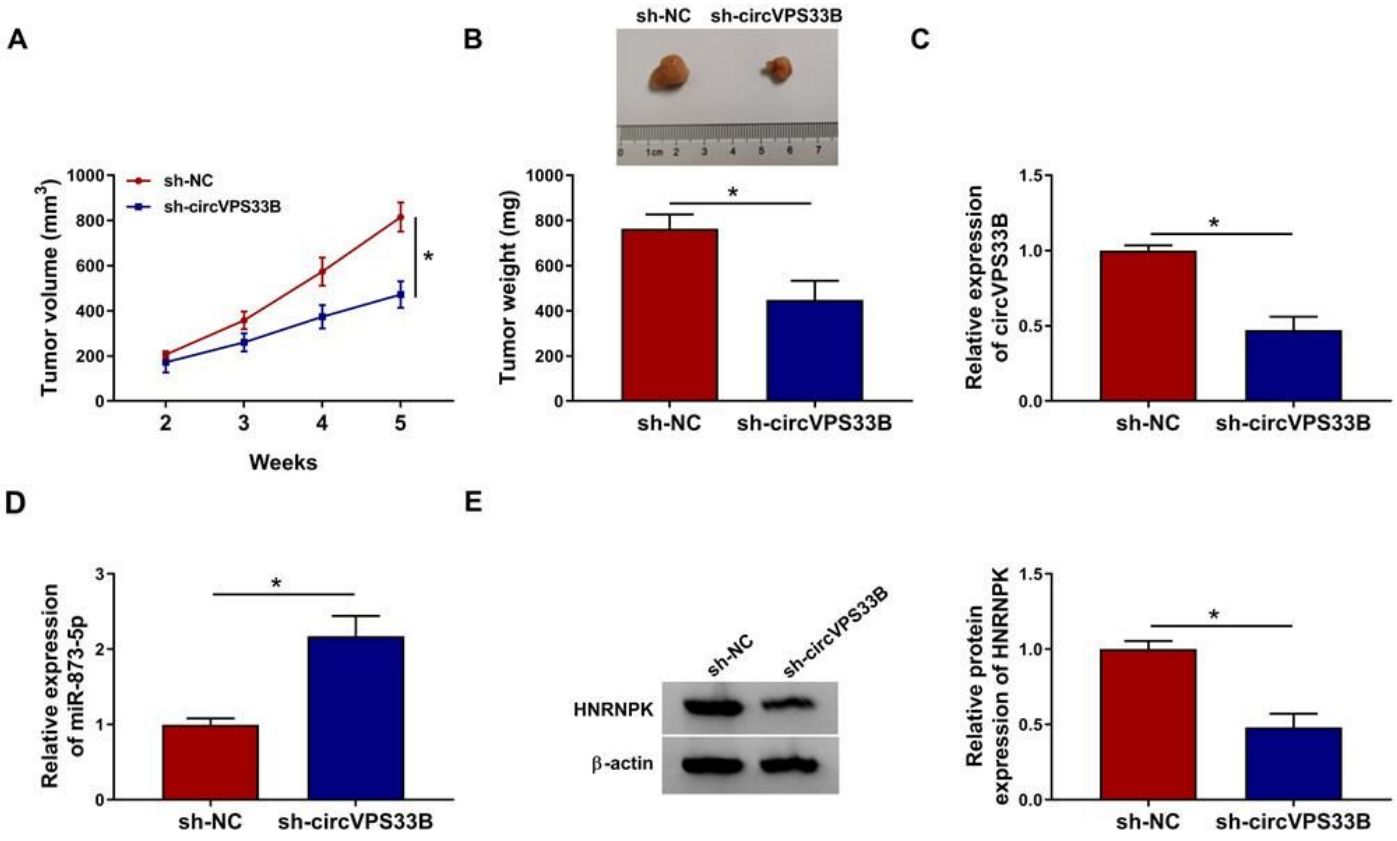

Figure 7

CircVPS33B silencing decreased the growth of infiltrative GC cells in vivo. (A and B) Tumor volume and weight were decreased in the sh-circVPS33B group compared to the control group. (C-E) QRT-PCR and western blotting were employed to analyze the levels of circVPS33B, miR-873-5p, or HNRNPK protein in mice tumor tissues of the sh-circVPS33B and sh-NC groups. *P < 0.05.